# Simulations of Liquid Crystals

Jeffrey Billeter, and Robert Pelcovits

Citation: Computers in Physics **12**, 440 (1998); doi: 10.1063/1.168726
View online: https://doi.org/10.1063/1.168726
View Table of Contents: https://aip.scitation.org/toc/cip/12/5
Published by the American Institute of Physics

# SIMULATIONS OF LIQUID CRYSTALS


## Jeffrey Billeter and Robert Pelcovits

**Department Editors:**
**Harvey Gould**
*hgould@clarku.edu*
**Jan Tobochnik**
*jant@kzoo.edu*


Liquid crystals are a class of materials that exhibit condensed phases with properties intermediate between those of solids and liquids. There is an incredibly diverse array of liquid-crystal phases, and the study of these phases is a multidisciplinary undertaking involving physicists, chemists, and engineers. With the advent of powerful computers, simulations have become an important tool for investigating models of liquid crystals, especially for understanding the link between molecular structure and the resulting macroscopic behavior.

In a solid, the centers of mass of the molecules fall on a lattice, and the molecular axes point in certain fixed directions—the solid is said to have both long-range positional and orientational order. A liquid has neither of these types of order. There may be some short-range clustering of molecules, but the molecular centers of mass diffuse freely, and the molecular axes point in random directions. Liquid-crystal phases fall somewhere between these two extremes, possessing orientational order and possibly some partial degree of positional order. To describe this situation, the term mesophases, meaning intermediate phases, is often used.

We first give some background on the various liquid-crystal phases and how the degree of order in these phases can be quantified. Next, we discuss how to set up a molecular-dynamics simulation using a well-established phenomenological model for liquid crystals, the Gay–Berne model. We also discuss some of the methods that can be used to assist in determining the structure of the phases.

The most common picture of an individual liquid-crystal molecule (often called a mesogen) is that of a rod, symmetric about its long axis.[1,2] Much about the essential types of phases and their nature can be understood with this simple model. More exotic phases require adding successive layers of refinement to the simple model, bringing the overall picture closer to the reality of the complex, underlying organic molecules. These refinements include, for example, adding flexible tails to the rod-shaped rigid cores[3] or adding transverse or longitudinal dipole moments.[4]

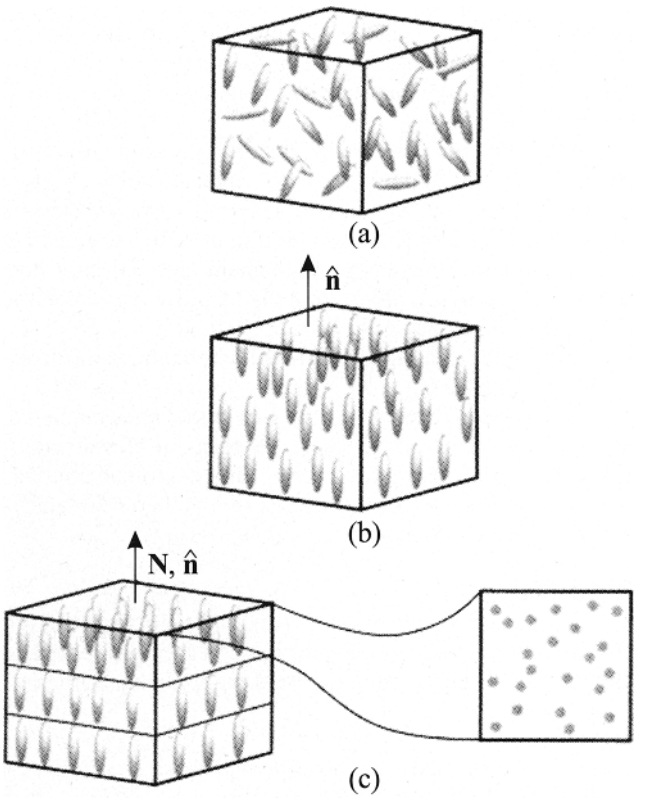


*Figure 1. Schematic representation of the position and orientation of anisotropic molecules in (a) the isotropic, (b) the nematic, and (c) the smectic A phases. The direction of average molecular alignment is specified by* $\hat{\mathbf{n}}$. *The layer normal in the smectic phase is indicated by* **N**. *Note that although the smectic layers are quite distinct in the figure, they tend to have a fair amount of interdigitation in practice.*

We focus on thermotropic liquid crystals: mesogens that form ordered phases as the temperature of the system is varied (in contrast to lyotropic liquid crystals, in which the mesogen concentration in solution determines the phases). If we begin with a completely disordered liquid (the isotropic phase) and cool the system, the simplest mesophase that can form is the nematic phase. In the nematic phase, the long axes of the molecules align with each other on average. However, the positional order is short-ranged like that of a conventional liquid (see Fig. 1).

The average direction of alignment is called the director $\hat{\mathbf{n}}$. Nematics have the property that $\hat{\mathbf{n}}$ is physically equivalent to $-\hat{\mathbf{n}}$. That is, the system can be rotated by 180° perpendicular to the director with no changes in physical properties. The degree of alignment along $\hat{\mathbf{n}}$ is described by an order parameter,


*Jeffrey Billeter is a graduate student in the Department of Physics, Brown University, Providence, RI 02912. E-mail: billeter@barus.physics.brown.edu*

*Robert Pelcovits is a professor in the Department of Physics, Brown University. E-mail: pelcovits@physics.brown.edu*



 S0894-1866(98)00705-6

$$S \equiv \langle P_2(\cos\theta) \rangle = \langle \tfrac{3}{2}\cos^2\theta - \tfrac{1}{2} \rangle, \tag{1}$$

where the brackets $\langle \cdots \rangle$ denote an ensemble average, $P_2$ is the second-order Legendre polynomial, and $\theta$ is the angle of the long molecular axis with respect to $\hat{\mathbf{n}}$. In the isotropic phase, $\langle \cos^2\theta \rangle = \frac{1}{3}$, and hence $S = 0$. As the system becomes more ordered, $S \to 1$. Note that a quantity such as $\langle \cos\theta \rangle$ would vanish because of the equivalence of the states $\hat{\mathbf{n}}$ and $-\hat{\mathbf{n}}$.

Upon further cooling, nematic phases can form smectic phases, in which the oriented molecules form a stack of two-dimensional layers (see Fig. 1). Within the layers, the molecular center-of-mass positions may be random (smectic *A*) or may form a hexatic phase (smectic *B*), in which each molecule is surrounded by six neighbors in a roughly hexagonal configuration. The hexagons all have the same orientation with respect to some fixed direction in the plane of the layers, but do not occupy sites consistent with any rigid, long-range lattice structure (see Fig. 2). The degree of this hexatic order (also known as bond-orientational order) is measured by the order parameter

$$\Psi = \langle e^{6i\theta_6} \rangle, \tag{2}$$

where $\theta_6$ is the angle between the vector connecting nearest neighbor molecules and some fixed axis in the plane of the layers. In more exotic smectic phases the molecules in the layers are tilted with respect to the normal to the layers (smectic *C*, *F*, and *I*).[1,2]

Liquid crystals can be simulated using either Monte Carlo or molecular dynamics (MD). We will describe how to do a MD simulation. The idea is to define an interaction potential for calculating forces and torques, write down the equations of motion, and then solve these equations numerically over a series of time steps to trace out the evolution of the system.

Much of the science and art of liquid-crystal simulations involves devising suitable models for the intermolecular pair potentials. An early approach, the Lebwohl–Lasher model,[5] neglected the translational degrees of freedom entirely by constraining the molecules to lattice sites and focused solely on the orientational interactions through the potential

$$-J \sum_{\langle ij \rangle} P_2(\hat{\mathbf{u}}_i \cdot \hat{\mathbf{u}}_j), \tag{3}$$

where $J$ is a coupling strength and $\hat{\mathbf{u}}_i$ is a unit vector along the long axis of molecule $i$. The sum is over all nearest-neighbor pairs in the system. Subsequent approaches (which allow for translational motion) include the use of both "hard" and "soft" interactions. Simulations of hard ellipsoids or, more commonly, hard spherocylinders (cylindrical rods with spherical caps at the ends) have yielded many valuable insights,[6] such as the fact that an anisotropic, repulsive potential with *no* attractive part is sufficient to produce a nematic phase. Smectic phases can be produced with spherocylinders, but not with ellipsoids.

The most widely used soft interaction is the Gay–Berne potential.[7] It is based on an extension of the simple Lennard-Jones 6–12 potential to model the anisotropic mesogenic shape. The complete Gay–Berne potential can be expressed as follows:

$$U(\hat{\mathbf{u}}_i, \hat{\mathbf{u}}_j, \mathbf{r}) = 4\varepsilon(\hat{\mathbf{u}}_i, \hat{\mathbf{u}}_j, \hat{\mathbf{r}}) \left[ \left( \frac{\sigma_0}{r - \sigma(\hat{\mathbf{u}}_i, \hat{\mathbf{u}}_j, \hat{\mathbf{r}}) + \sigma_0} \right)^{12} - \left( \frac{\sigma_0}{r - \sigma(\hat{\mathbf{u}}_i, \hat{\mathbf{u}}_j, \hat{\mathbf{r}}) + \sigma_0} \right)^{6} \right], \tag{4}$$

where $\mathbf{r}$ is the intermolecular distance $\mathbf{r} = \mathbf{r}_i - \mathbf{r}_j$, $r = |\mathbf{r}|$, $\hat{\mathbf{r}} = \mathbf{r}/r$, and $\sigma_0$ sets the length scale for the potential. The parameter $\sigma(\hat{\mathbf{u}}_i, \hat{\mathbf{u}}_j, \hat{\mathbf{r}})$ is the intermolecular separation at which the potential vanishes and hence represents the shape of the molecules. Its explicit form is

$$\sigma(\hat{\mathbf{u}}_i, \hat{\mathbf{u}}_j, \hat{\mathbf{r}}) = \sigma_0 \left[ 1 - \frac{1}{2}\chi_\sigma \left( \frac{(\hat{\mathbf{r}} \cdot \hat{\mathbf{u}}_i + \hat{\mathbf{r}} \cdot \hat{\mathbf{u}}_j)^2}{1 + \chi_\sigma \hat{\mathbf{u}}_i \cdot \hat{\mathbf{u}}_j} + \frac{(\hat{\mathbf{r}} \cdot \hat{\mathbf{u}}_i - \hat{\mathbf{r}} \cdot \hat{\mathbf{u}}_j)^2}{1 - \chi_\sigma \hat{\mathbf{u}}_i \cdot \hat{\mathbf{u}}_j} \right) \right]^{-1/2}, \tag{5}$$

where $\chi_\sigma$ is

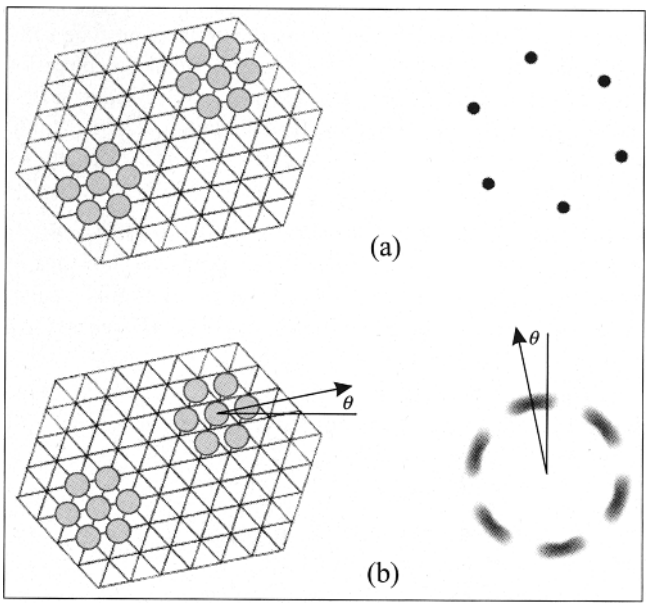


*Figure 2. Separated groups of nearest-neighbor atoms in (a) a hexagonal crystalline phase and (b) a hexatic phase. In (a) and (b), each atom has six nearest neighbors forming a local hexagon and distant hexagons have the same orientation relative to some fixed axis. In (b), however, the atoms do not occupy sites of a triangular lattice as in (a). Figures 1 and 2 are reprinted by permission from Ref. 1, Figs. 2.7.3 and 2.7.8, respectively.*

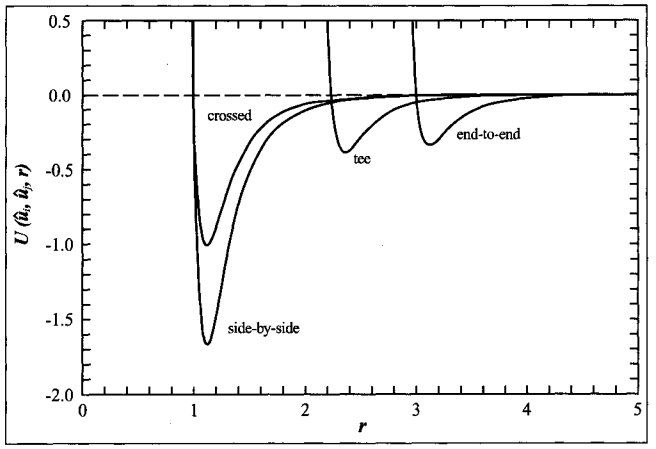


*Figure 3. The distance dependence of the Gay–Berne potential energy in Eq. (4) for four orientations of the molecules with respect to each other and to their intermolecular vector. The four orientations correspond to* $\hat{\mathbf{u}}_i\cdot\hat{\mathbf{u}}_j=1$, $\hat{\mathbf{r}}\cdot\hat{\mathbf{u}}_i=\hat{\mathbf{r}}\cdot\hat{\mathbf{u}}_j=0$ *(side-by-side),* $\hat{\mathbf{u}}_i\cdot\hat{\mathbf{u}}_j=0$, $\hat{\mathbf{r}}\cdot\hat{\mathbf{u}}_i=\hat{\mathbf{r}}\cdot\hat{\mathbf{u}}_j=0$ *(crossed),* $\hat{\mathbf{u}}_i\cdot\hat{\mathbf{u}}_j=0$, $\hat{\mathbf{r}}\cdot\hat{\mathbf{u}}_i=0$, $\hat{\mathbf{r}}\cdot\hat{\mathbf{u}}_j=1$ *(tee), and* $\hat{\mathbf{u}}_i\cdot\hat{\mathbf{u}}_j=1$, $\hat{\mathbf{r}}\cdot\hat{\mathbf{u}}_i=\hat{\mathbf{r}}\cdot\hat{\mathbf{u}}_j=1$ *(end-to-end). The exponents are* $\mu=2$ *and* $\nu=1$. *The energy is measured in terms of* $\epsilon_0$ *and distance in units of* $\sigma_0$. *Note that when* $\sigma>1+2^{1/6}$, *the Gay–Berne potential has an additional minimum at a smaller value of r. In practice, these additional minima are irrelevant, because they are separated from those shown by infinite barriers.*

$$\chi_\sigma=\frac{(\sigma_e/\sigma_s)^2-1}{(\sigma_e/\sigma_s)^2+1}. \tag{6}$$

Here $\sigma_e$ is the separation between two molecules when they are oriented end-to-end, and $\sigma_s$ is the separation when the molecules are side-by-side. For a spherically symmetric molecule $(\sigma_e/\sigma_s)=1$, $\chi_\sigma=0$, and Eq. (5) reduces to the usual Lennard-Jones potential. If two molecules are lined up side by side, then $\hat{\mathbf{r}}\cdot\hat{\mathbf{u}}_j=\hat{\mathbf{r}}\cdot\hat{\mathbf{u}}_i=0$, and $\sigma(\hat{\mathbf{u}}_i,\hat{\mathbf{u}}_j,\hat{\mathbf{r}})=\sigma_0$. The potential will then vanish at $r=\sigma_0$. If two molecules are lined up end to end, then $\hat{\mathbf{r}}\cdot\hat{\mathbf{u}}_j=\hat{\mathbf{r}}\cdot\hat{\mathbf{u}}_i=\hat{\mathbf{u}}_i\cdot\hat{\mathbf{u}}_j=1$, and $\sigma(\hat{\mathbf{u}}_i,\hat{\mathbf{u}}_j,\hat{\mathbf{r}})=\sigma_0\sigma_e/\sigma_s$. The potential vanishes at $r=\sigma_0\sigma_e/\sigma_s$. It is convenient to have the potential vanish at $\sigma_s$ and $\sigma_e$ for these two cases, and hence we set $\sigma_0=\sigma_s$.

The quantity $\varepsilon(\hat{\mathbf{u}}_i,\hat{\mathbf{u}}_j,\hat{\mathbf{r}})$ is the well depth and represents the anisotropy of the attractive interactions. The well depth is written as

$$\varepsilon(\hat{\mathbf{u}}_i,\hat{\mathbf{u}}_j,\hat{\mathbf{r}})=\varepsilon_0\,\varepsilon^\nu(\hat{\mathbf{u}}_i,\hat{\mathbf{u}}_j)g_\epsilon^\mu(\hat{\mathbf{u}}_i,\hat{\mathbf{u}}_j,\hat{\mathbf{r}}), \tag{7}$$

where

$$\varepsilon(\hat{\mathbf{u}}_i,\hat{\mathbf{u}}_j)=[1-\chi_\sigma^2(\hat{\mathbf{u}}_i\cdot\hat{\mathbf{u}}_j)^2]^{-1/2}, \tag{8}$$

and

$$g_\epsilon(\hat{\mathbf{u}}_i,\hat{\mathbf{u}}_j,\hat{\mathbf{r}})=1-\frac{1}{2}\chi_\epsilon\left(\frac{(\hat{\mathbf{r}}\cdot\hat{\mathbf{u}}_i+\hat{\mathbf{r}}\cdot\hat{\mathbf{u}}_j)^2}{1+\chi_\epsilon\hat{\mathbf{u}}_i\cdot\hat{\mathbf{u}}_j}+\frac{(\hat{\mathbf{r}}\cdot\hat{\mathbf{u}}_i-\hat{\mathbf{r}}\cdot\hat{\mathbf{u}}_j)^2}{1-\chi_\epsilon\hat{\mathbf{u}}_i\cdot\hat{\mathbf{u}}_j}\right), \tag{9}$$

with $\chi_\epsilon$ defined in terms of $\varepsilon_e$ and $\varepsilon_s$, the end-to-end and side-by-side well depths, respectively, as

$$\chi_\epsilon=\frac{1-(\varepsilon_e/\varepsilon_s)^{1/\mu}}{1+(\varepsilon_e/\varepsilon_s)^{1/\mu}}. \tag{10}$$

Without the introduction of $g_\epsilon$, the well depths for all orientations would be the same. To model the more realistic variation of well depth with orientation, the factor $g_\epsilon\sim 1/\sigma^2$ is added, but with a new parameter $\chi_\epsilon$ that allows fine control over the actual spread of well depths.

All the parameters are freely adjustable (although not all values will yield mesophases). Commonly used values are $\mu=2$, $\nu=1$, $\sigma_e/\sigma_s=3$, and $\varepsilon_s/\varepsilon_e=5$; $\varepsilon_0$ can be adjusted to set an overall energy scale. These values have allowed the successful simulation of nematic, smectic *A*, and smectic *B* phases.[8] Note that if we choose $\sigma_s>\sigma_e$, then we can model disc-shaped molecules, leading to discotic liquid-crystal phases, in which the axes normal to the discs are aligned.[9] Figure 3 shows the Gay–Berne potential (using the parameters shown above) for four molecular configurations.

In the same figure, we can see that all the curves are essentially zero for separations $r/\sigma_0$ greater than about four. Thus, as is typical in most simulations, the value four (or a value close to it) can be used as a potential cutoff, meaning that only those particles with center-of-mass separations of four or less will be considered for calculations of the potential energy, force, and torque. This approximation allows an enormous savings in computation time.

As alluded to above, it is common to use reduced units.[10] The assignments $\sigma_0=1$, $\varepsilon_0=1$, and $m=1$ (where $m$ is particle mass) allow all dimensional quantities to be expressed in terms of $\sigma_0$, $\varepsilon_0$, and $m$ or their combinations. For example, the time in MD simulations is measured in units of $\sqrt{m\sigma_0^2/\varepsilon_0}$.

A computationally efficient scheme for tracking the orientations of the molecules must be used, because the molecules are not isotropic as are hard spheres; quaternions are typically used for this purpose.[11] Although quaternions appear naturally in group theory and complex algebra,[12] we use them here simply for convenience and efficiency. A more intuitive approach might make use of Euler angles, but the appearance of many trigonometric functions would introduce a heavy computational expense. Furthermore, the equations of motion for the Euler angles include trigonometric functions in denominators in several places, yielding the dangerous possibility of floating-point exceptions. The

quaternion approach suffers from neither of these difficulties.

A quaternion $\mathbf{Q}$ is a set of four scalar quantities:

$$\mathbf{Q}=(q_0,q_1,q_2,q_3), \tag{11}$$

with the constraint $\Sigma_{i=0}^{3}q_i^2=1$. The components $q_i$ can be defined in terms of Euler angles, allowing the more intuitive Euler-angle equations to be recast in terms of quaternions. For example, the rotation matrix $\mathbf{R}$, which rotates a vector in the instantaneous body frame of a molecule to a fixed space frame, is given by

$$\mathbf{R}=\begin{pmatrix} q_0^2+q_1^2-q_2^2-q_3^2 & 2(-q_0q_3+q_1q_2) & 2(q_0q_2+q_1q_3) \\ 2(q_0q_3+q_1q_2) & q_0^2-q_1^2+q_2^2-q_3^2 & 2(-q_0q_1+q_2q_3) \\ 2(-q_0q_2+q_1q_3) & 2(q_0q_1+q_2q_3) & q_0^2-q_1^2-q_2^2+q_3^2 \end{pmatrix} \tag{12}$$

This relation corresponds to Eq. (4-47) in Ref. 12.

The Gay–Berne potential is defined in terms of the vectors $\hat{\mathbf{u}}$, not quaternions. A simple way to determine $(u_x,u_y,u_z)$ from the $q_i$ is to use $\mathbf{R}$ to rotate the vector $\hat{\mathbf{u}}_b=(0,0,1)$ (a unit vector along the long axis in the body frame) into the space frame. That is,

$$\hat{\mathbf{u}}=\mathbf{R}\hat{\mathbf{u}}_b. \tag{13}$$

Of course, this rotation needs to be done for each molecule in the system.

We can now write the equations of motion explicitly. Straightforward Hamiltonian dynamics for the translational degrees of freedom yields for each particle $i=1,\ldots,N$:

$$\dot{\mathbf{r}}_i=\mathbf{p}_i \tag{14a}$$

$$\dot{\mathbf{p}}_i=-\frac{\partial U}{\partial \mathbf{r}_i}, \tag{14b}$$

where $\mathbf{p}$ is the particle momentum (recall that $m=1$), and $U$ is the sum over all possible pair potentials of the form Eq. (4).

The equations for the orientational degrees of freedom look much more complicated than those for the translational degrees of freedom, but are derived from Hamiltonian dynamics with the constraint $\Sigma_i q_i^2=1$ for each particle. They can be written as:

$$\begin{pmatrix} \dot{q}_0 \\ \dot{q}_1 \\ \dot{q}_2 \\ \dot{q}_3 \end{pmatrix}=\frac{1}{2}\begin{pmatrix} q_0 & -q_1 & -q_2 & -q_3 \\ q_1 & q_0 & -q_3 & q_2 \\ q_2 & q_3 & q_0 & -q_1 \\ q_3 & -q_2 & q_1 & q_0 \end{pmatrix}\begin{pmatrix} 0 \\ \omega_x \\ \omega_y \\ \omega_z \end{pmatrix}, \tag{15}$$

$$\dot{S}_{i\alpha}=\sum_{\beta,\gamma}\epsilon_{\alpha\beta\gamma}\frac{S_{i\beta}S_{i\gamma}}{I_\gamma}+\tau_{i\alpha}, \tag{16}$$

where $\tau$ is the torque and the instantaneous-body-frame angular velocity $\omega$ is $\omega_{i\alpha}=S_{i\alpha}/I_\alpha$, with $S_{i\alpha}$ a component of the angular momentum and $I_\alpha$ the diagonal elements of the moment of inertia. Possible values are $(I_x,I_y,I_z)=(0.5,0.5,0.25)$, although these values may be adjusted as well. Note that the equations for the $\dot{S}_i$ are simply the standard Euler equations.[12]

The torque on molecule $i$ in the space frame can be computed in terms of the generalized force $-\nabla_{\hat{\mathbf{u}}}U$ using the relation:

$$\boldsymbol{\tau}_i=\hat{\mathbf{u}}_i\times(-\nabla_{\hat{\mathbf{u}}}\mathbf{U}). \tag{17}$$

In the instantaneous body frame we find for molecule $i$ (omitting the subscript $i$ for clarity), using Eqs. (12), (13), and (17):

$$\tau_x=2(q_1q_2-q_0q_3)\frac{\partial U}{\partial u_x}+(q_0^2-q_1^2+q_2^2-q_3^2)\frac{\partial U}{\partial u_y}+2(q_0q_1+q_2q_3)\frac{\partial U}{\partial u_z}, \tag{18a}$$

$$\tau_y=(-q_0^2-q_1^2+q_2^2+q_3^2)\frac{\partial U}{\partial u_x}+2(-q_0q_3-q_1q_2)\frac{\partial U}{\partial u_y}+2(q_0q_2-q_1q_3)\frac{\partial U}{\partial u_z}, \tag{18b}$$

$$\tau_z=0. \tag{18c}$$

The equation $\tau_z=0$ indicates that in the present model, which has uniaxial symmetry, a molecule can rotate freely about its long axis.

We now give the explicit equations for the partial derivatives of $U$.[13] To simplify the notation, we define

$$R=[\mathbf{r}-\sigma(\hat{\mathbf{u}}_i,\hat{\mathbf{u}}_j,\hat{\mathbf{r}})+\sigma_0]/\sigma_0, \tag{19}$$

and

$$g_\sigma^{-1/2}=\sigma(\hat{\mathbf{u}}_i,\hat{\mathbf{u}}_j,\hat{\mathbf{r}})/\sigma_0. \tag{20}$$

If we write $x$ for $r_{ix}$, we have for example,

$$\frac{\partial U}{\partial x}=4\varepsilon_0\left(\varepsilon^\nu(\hat{\mathbf{u}}_i,\hat{\mathbf{u}}_j)\,g_\epsilon^\mu(6R^{-7}-12R^{-13})\frac{\partial R}{\partial x}+(R^{-12}-R^{-6})\varepsilon^\nu(\hat{\mathbf{u}}_i,\hat{\mathbf{u}}_j)\,\mu g_\epsilon^{\mu-1}\frac{\partial g_\epsilon}{\partial x}\right), \tag{21}$$

where

$$\frac{\partial R}{\partial x}=\frac{x}{\sigma_0 r}+\frac{1}{2}g_\sigma^{-3/2}\frac{\partial g_\sigma}{\partial x}, \tag{22}$$

$$\frac{\partial g_\rho}{\partial x} = -\frac{\chi_\rho}{r}\left(\frac{\hat{\mathbf{r}}\cdot\hat{\mathbf{u}}_i+\hat{\mathbf{r}}\cdot\hat{\mathbf{u}}_j}{1+\chi_\rho\hat{\mathbf{u}}_i\cdot\hat{\mathbf{u}}_j}(\hat{u}_{ix}+\hat{u}_{jx}) + \frac{\hat{\mathbf{r}}\cdot\hat{\mathbf{u}}_i-\hat{\mathbf{r}}\cdot\hat{\mathbf{u}}_j}{1-\chi_\rho\hat{\mathbf{u}}_i\cdot\hat{\mathbf{u}}_j}(\hat{u}_{ix}-\hat{u}_{jx})\right) + \frac{x\chi_\rho}{r^2}\left(\frac{(\hat{\mathbf{r}}\cdot\hat{\mathbf{u}}_i+\hat{\mathbf{r}}\cdot\hat{\mathbf{u}}_j)^2}{1+\chi_\rho\hat{\mathbf{u}}_i\cdot\hat{\mathbf{u}}_j}+\frac{(\hat{\mathbf{r}}\cdot\hat{\mathbf{u}}_i-\hat{\mathbf{r}}\cdot\hat{\mathbf{u}}_j)^2}{1-\chi_\rho\hat{\mathbf{u}}_i\cdot\hat{\mathbf{u}}_j}\right). \quad (23)$$

The quantity $\chi_\rho$ can be set to $\chi_\sigma$ or $\chi_\epsilon$ for $g_\sigma$ defined in Eq. (20) or $g_\epsilon$ defined in Eq. (9), respectively.[14] By using Newton's third law, we find that only half the force pairs need to be explicitly calculated. Unfortunately, such a simple relation does not hold for the torques, because the forces are not central.

For computing the torques we have the generalized forces:

$$\frac{\partial U}{\partial \hat{u}_{ix}} = 4(R^{-12}-R^{-6})\frac{\partial \varepsilon(\hat{\mathbf{u}}_i,\hat{\mathbf{u}}_j,\hat{\mathbf{r}})}{\partial \hat{u}_{ix}} + 4\varepsilon(\hat{\mathbf{u}}_i,\hat{\mathbf{u}}_j,\hat{\mathbf{r}})(6R^{-7}-12R^{-13})\frac{\partial R}{\partial \hat{u}_{ix}}, \quad (24)$$

where

$$\frac{\partial \varepsilon(\hat{\mathbf{u}}_i,\hat{\mathbf{u}}_j,\hat{\mathbf{r}})}{\partial \hat{u}_{ix}} = \varepsilon_0\,\varepsilon^{\nu}(\hat{\mathbf{u}}_i,\hat{\mathbf{u}}_j)\,\mu g_\epsilon^{\mu-1}\frac{\partial g_\epsilon}{\partial \hat{u}_{ix}} + \varepsilon_0\nu\varepsilon^{\nu-1}(\hat{\mathbf{u}}_i,\hat{\mathbf{u}}_j)g_\epsilon^{\mu}\frac{\partial \varepsilon(\hat{\mathbf{u}}_i,\hat{\mathbf{u}}_j)}{\partial \hat{u}_{ix}}, \quad (25)$$

$$\frac{\partial \varepsilon(\hat{\mathbf{u}}_i,\hat{\mathbf{u}}_j)}{\partial \hat{u}_{ix}} = \chi_\sigma^2\varepsilon^3(\hat{\mathbf{u}}_i,\hat{\mathbf{u}}_j)(\hat{\mathbf{u}}_i\cdot\hat{\mathbf{u}}_j)\hat{u}_{jx}, \quad (26)$$

$$\frac{\partial R}{\partial \hat{u}_{ix}} = \frac{1}{2}\left(\frac{\sigma(\hat{\mathbf{u}}_i,\hat{\mathbf{u}}_j,\hat{\mathbf{r}})}{\sigma_0}\right)^3\frac{\partial g_\sigma}{\partial \hat{u}_{ix}}, \quad (27)$$

and

$$\frac{\partial g_\rho}{\partial \hat{u}_{ix}} = -\chi_\rho\left[\hat{r}_x\left(\frac{\hat{\mathbf{r}}\cdot\hat{\mathbf{u}}_i+\hat{\mathbf{r}}\cdot\hat{\mathbf{u}}_j}{1+\chi_\rho\hat{\mathbf{u}}_i\cdot\hat{\mathbf{u}}_j}+\frac{\hat{\mathbf{r}}\cdot\hat{\mathbf{u}}_i-\hat{\mathbf{r}}\cdot\hat{\mathbf{u}}_j}{1-\chi_\rho\hat{\mathbf{u}}_i\cdot\hat{\mathbf{u}}_j}\right) + \frac{\chi_\rho}{2}\hat{u}_{jx}\left(\frac{(\hat{\mathbf{r}}\cdot\hat{\mathbf{u}}_i-\hat{\mathbf{r}}\cdot\hat{\mathbf{u}}_j)^2}{(1-\chi_\rho\hat{\mathbf{u}}_i\cdot\hat{\mathbf{u}}_j)^2}-\frac{(\hat{\mathbf{r}}\cdot\hat{\mathbf{u}}_i+\hat{\mathbf{r}}\cdot\hat{\mathbf{u}}_j)^2}{(1+\chi_\rho\hat{\mathbf{u}}_i\cdot\hat{\mathbf{u}}_j)^2}\right)\right]. \quad (28)$$

Before discussing the solution of the equations of motion, we mention another time-saving technique. If we introduce a potential cutoff, it would save time to check only those pairs of molecules that are likely to have separations near or less than the cutoff. One way of doing so is to use a neighbor list.[10] If the cutoff separation is 4.0, then for each molecule we create a list of its surrounding neighbors that have separations of, say, 4.4. Because the molecules change their separations rather slowly (we must choose a small enough time step to solve the equations of motion accurately), only the molecules on this list need to be checked to see if they fall within the cutoff. The neighbor list needs to be updated every 10 steps or so.

The equations of motion are fairly simple differential equations and could, in principle, be solved numerically by standard methods such as the Runge–Kutta method. However, in practice, such methods are hardly ever used because they would require several evaluations of all the forces and torques for each time step, and the computational expense would be enormous. A method known as the leapfrog algorithm is widely used and will be described in the next paragraph.[10]

*The equations of motion are fairly simple differential equations and could, in principle, be solved numerically by standard methods.*

Suppose we know the positions and orientations at time $t$ and the momenta at time $t-\Delta t/2$, where $\Delta t$ is the MD time step, typically 0.001 in reduced units. The forces at time $t$ can be calculated and then used to advance the momenta to time $t+\Delta t/2$ by the following equation:

$$p(t+\tfrac{1}{2}\Delta t) = p(t-\tfrac{1}{2}\Delta t)+F(t)\,\Delta t. \quad (29)$$

Once the $p(t+\frac{1}{2}\Delta t)$ are known, they can be used to advance the positions using:

$$x(t+\Delta t) = x(t)+p(t+\tfrac{1}{2}\Delta t)\,\Delta t. \quad (30)$$

The positions and momenta continue leapfrogging over each other (hence the name of the algorithm) for as many steps as desired.

We often want to know the values of all variables at the same time $t$. To obtain $p(t)$, we compute

$$p(t) = p(t-\tfrac{1}{2}\Delta t)+\tfrac{1}{2}F(t)\Delta t,$$

or equivalently

$$p(t) = \tfrac{1}{2}[p(t-\tfrac{1}{2}\Delta t)+p(t+\tfrac{1}{2}\Delta t)]. \quad (31)$$

The orientational equations are trickier, because of the functional dependence of the variable derivatives on the variables themselves. A slightly modified leapfrog scheme

with convergence loops is used.[15] For the angular momentum, we want ultimately to advance from $t-\Delta t/2$ to $t+\Delta t/2$ using

$$S(t+\tfrac{1}{2}\Delta t)=S(t-\tfrac{1}{2}\Delta t)+\dot{S}[S(t),\tau(t)]\Delta t. \quad (32)$$

We do not know $S(t)$, but we can calculate it iteratively using

$$S(t)=S(t-\tfrac{1}{2}\Delta t)+\tfrac{1}{2}\dot{S}[\tilde{S}(t),\tau(t)]\Delta t, \quad (33)$$

where initially we set $\tilde{S}(t)=S(t-\frac{1}{2}\Delta t)$. The value obtained for $S(t)$ is then returned to Eq. (33) as $\tilde{S}(t)$, and a new $S(t)$ is calculated. After a few iterations, a self-consistent solution is obtained. Note that $\tau(t)$ is used in each iteration and never recalculated. Once $S(t)$ is known, it can be used in Eq. (32) to fully advance the angular momentum.

A similar approach is used for the quaternions. Ultimately, we want

$$q(t+\Delta t)=q(t)+q[q(t+\tfrac{1}{2}\Delta t),\ S(t+\tfrac{1}{2}\Delta t)]\Delta t. \quad (34)$$

Having obtained $S(t+\frac{1}{2}\Delta t)$ already, we simply need to calculate an iterative solution for $q(t+\Delta t/2)$ using

$$q(t+\tfrac{1}{2}\Delta t)=q(t)+\tfrac{1}{2}\dot{q}[\tilde{q}(t+\tfrac{1}{2}\Delta t),\ S(t+\tfrac{1}{2}\Delta t)]\Delta t. \quad (35)$$

Again, the initial guess for $\tilde{q}(t+\Delta t/2)$ is $q(t)$. The value obtained for $q(t+\Delta t/2)$ is returned to Eq. (35) as $\tilde{q}(t+\Delta t/2)$, and a new $q(t+\Delta t/2)$ is calculated. A self-consistent solution, which is obtained after a few iterations, can then be used in Eq. (34) to advance the quaternions fully.

We can determine dynamically the number of iterations by explicitly checking for convergence. Alternatively, we could simply use a sufficiently large but fixed number of iterations. For the simulation parameters described here, five iterations in each of the two convergence loops should be sufficient.

How do we know that the equations of motion are being solved accurately? Molecular dynamics offers a strong check in that the total energy of the system

$$E=U+\frac{1}{2}\sum_{i,\alpha} p_{i,\alpha}^2+\frac{1}{2}\sum_{i,\alpha}\frac{S_{i,\alpha}^2}{I_\alpha} \quad (36)$$

should be conserved.[10] We should calculate $E$ at regular intervals and check that it remains fixed to within 1 part in $10^4$ over tens and even hundreds of thousands of time steps. If $E$ is not being conserved, there is an error either in the algorithm or in the force and torque calculations. Of course, $E$ should be calculated using the values of all the variables at the same time.

The simulation we are describing corresponds to the microcanonical ensemble, that is, the constant $NVE$ ensemble. The number of molecules $N$ is chosen in advance—we will use $N=256$ in the projects described later. The volume $V$ is usually set indirectly by choosing a desired number density $\rho$ and calculating $V=N/\rho$. The simulation volume is usually chosen to be cubic, so the length of each side is $L=\sqrt[3]{N/\rho}$. Various techniques can be used to simulate constant-temperature and constant-pressure ensembles.[16]

Two other points regarding the details of the simulation need to be discussed: periodic boundary conditions and the minimum-image convention.[10] In simulations of the bulk behavior of a system, the effects of boundaries need to be minimized or completely eliminated. With any system size that can be simulated within reasonable time and memory constraints, the boundary effects would be much too large; the use of periodic boundary conditions effectively removes all boundaries.

Imagine the system of interest to be contained within a cube that is exactly replicated an infinite number of times on all sides. If a molecule exits the central cube through the top, then the molecule's exact image simultaneously enters the cube through the bottom. The actual positions are always in the central cube, but the molecules remain completely free to move without any interactions with boundary surfaces.

After applying Eq. (30) and before computing the new forces and torques, we must apply the periodic boundary conditions as follows:

$$\text{if } (x>L/2) \text{ then } x=x-L, \quad (37a)$$

$$\text{if } (x<-L/2) \text{ then } x=x+L. \quad (37b)$$

This procedure is carried out for the $x$, $y$, and $z$ components of the positions of all molecules. If we were to use a more general box shape instead of a cube (as is the case in two the project configurations described below), we would use the appropriate box length for the $x$, $y$, or $z$ direction in place of the general $L$ in Eqs. (37) and (38) below.

Closely related to the use of periodic boundary conditions is the minimum-image convention. In principle, all the replicated images must be considered when calculating the neighbor list. In practice, the potential cutoff allows one to consider only the nearest image (the *minimum* image). This scheme is implemented in a manner similar to the periodic-boundary-condition scheme:

$$\text{if } (x_{ij}>L/2) \text{ then } x_{ij}=x_{ij}-L, \quad (38a)$$

$$\text{if } (x_{ij}<-L/2) \text{ then } x_{ij}=x_{ij}+L. \quad (38b)$$

This procedure is carried out for the $x$, $y$, and $z$ components of the intermolecular separations of all pairs in the system. (Actually, only half the pairs need to be considered because $\mathbf{r}_{ij}=-\mathbf{r}_{ji}$.) Note that the cutoff must be less than half the cube side, and so there is an upper limit on the densities that can be simulated for a given set of potential parameters.

The nematic order parameter $S$ is given by the largest eigenvalue of the tensor order parameter:[1]

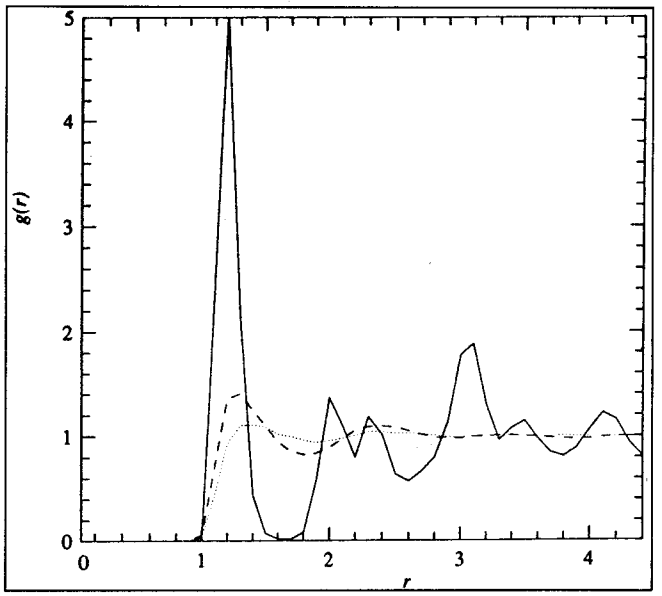


*Figure 4. The orientationally averaged radial distribution function for the isotropic (···), nematic (– – –), and smectic B (—) phases. The dimensionless quantity r is measured in terms of the parameter $\sigma_0$.*

$$Q_{\alpha\beta}=\frac{1}{N}\sum_i (3u_{i\alpha}u_{i\beta}-\delta_{\alpha\beta})/2, \tag{39}$$

where $\alpha=x,y,z$. The eigenvector corresponding to $S$ is $\hat{\mathbf{n}}$. In the ordered phases, both $S$ and $\hat{\mathbf{n}}$ may fluctuate considerably, but they should be distinctly different from the values in the less ordered phases. The fluctuations are partly due to the small number of molecules; this small number also implies that $S$ for the isotropic phase is nonzero, although small.

To obtain the bond-orientational order parameter $\Psi$ in the hexatic phase, we compute

$$\Psi=\left|\left\langle\frac{1}{N}\sum_i \frac{1}{n_i}\sum_{\langle j\rangle} e^{6i\theta_{ij}}\right\rangle\right|, \tag{40}$$

where $n_i$ is the number of pairs of nearest neighbors (defined later) of the $i$th molecule, $\langle j\rangle$ indicates a sum over all those nearest neighbors, and $\theta_{ij}$ is the angle between the projection onto the plane perpendicular to the director of the vector connecting molecules $i$ and $j$ (for example, $\mathbf{r}_{ij}-\mathbf{r}_{ij}\cdot\hat{\mathbf{n}}$) and some fixed direction in that plane (see Fig. 2). When we compute $S$ and $\hat{\mathbf{n}}$ from Eq. (39), we usually can obtain all the eigenvectors simultaneously. These three vectors define a coordinate system with the director as one of the axes. The "fixed" direction needed for calculating $\Psi$ can be chosen as one of the other two eigenvectors in this director-based coordinate system.

The definition of nearest neighbors as well as further insights into the structure of the phases can be obtained by computing the radial distribution functions.[9] The orientationally averaged radial distribution function $g(r)$ measures the average probability per molecule, relative to that in an ideal gas, of finding another molecule at a separation $r$:

$$g(r)=\frac{\langle n(r)\rangle}{\langle n_{\text{ideal}}(r)\rangle}. \tag{41}$$

First, a set of bins for the intermolecular separations is created. The bins can extend out to half the box length $L$ with bin widths of, say, 0.1. The average ideal-gas density $\langle n_{\text{ideal}}(r)\rangle$ is simply a constant $\rho=N/V$. The average density $\langle n(r)\rangle$ is calculated by distributing all the pair separations in the system into appropriate bins and then dividing the value obtained for each bin by the volume of the spherical shell associated with it. A final division by $N$ normalizes $g(r)$ to a per-molecule function. Thus,

$$g(r)=\frac{1}{N\rho}\sum_i \sum_{j\neq i} \frac{\delta(r-r_{ij})}{\frac{4}{3}\pi[(r+\Delta r)^3-r^3]}, \tag{42}$$

where $\Delta r$ is the bin width and the $\delta$ function is equal to 1 if $r_{ij}$ falls within the bin centered on $r$ and is zero otherwise.

Figure 4 shows $g(r)$ for the isotropic ($I$), nematic ($N$), and smectic $B$ (Sm $B$) phases. Note that $g(r)$ is essentially zero for small $r$, indicating that there is little interpenetration of the soft molecules. At somewhat larger values of $r$, $g(r)$ has a noticeable maximum, indicating the presence of short-ranged clustering. In the $I$ phase, $g(r)$ shows little further structure for larger values of $r$ and remains essentially constant at the value 1, indicating that there is only very short-ranged order. The effect of the pair potential is negligible beyond a short intermolecular separation, and the molecules behave essentially like an ideal gas. The minimum in $g(r)$ following the first peak defines the limit of

**Table. The format of pre-equilibrated configurations that can be downloaded from ftp://ftp.aip.org/cip/cip_sourcecode/billeter_so_98/. The names of the files are isot.dat, nem.dat, smA.dat, and smB.dat.**

| Line | Content |
|---|---|
| 1 | positions and orientations (text) |
| 2–257 | Each line gives the positions $x$, $y$, $z$ and the orientations $q_0$, $q_1$, $q_2$, $q_3$ of a molecule |
| 258 | momenta (text) |
| 259–514 | Each line gives the momenta $p_x$, $p_y$, $p_z$ and the angular momenta $S_x$, $S_y$, $S_z$ of a molecule |
| 515 | thermodynamic quantities (text) |
| 516 | translational temperature |
| 517 | rotational temperature |
| 518 | pressure |
| 519 | potential energy |
| 520 | total energy (conserved) |
| 521 | density |
| 522 | simulation box dimensions $L_x$, $L_y$, $L_z$ |
| 523 | $S$, $\Psi$ |
| 524 | the director components $n_x$, $n_y$, $n_z$ |

short-ranged clustering; this limit is often referred to as the first coordination shell and defines the meaning of nearest neighbors in our definition of $\Psi$ in Eq. (40). Note that the $N$ and Sm $B$ phases show stronger short-ranged ordering than in the $I$ phase. There are also additional peaks, which are indicative of the one-dimensional long-ranged translational order in the smectic $B$ phase and the precursors to that order in the $N$ phase.

The distribution function parallel to the director $g_{\parallel}(r_{\parallel})$ provides a clear indication of smectic ordering (see Fig. 5). The parallel distribution function is calculated in a manner similar to the calculation for $g(r)$, but the intermolecular separations $\mathbf{r}$ are projected onto the director $\hat{\mathbf{n}}$ and the bins are created for these projections $r_{\parallel}$:

$$g_{\parallel}(r_{\parallel})=\frac{1}{N\rho}\sum_i \sum_{j\neq i} \frac{\delta(r_{\parallel}-r_{\parallel,ij})}{2L^2\Delta r_{\parallel}}. \tag{43}$$

The $\delta$ function is again equal to 1 for $r_{\parallel,ij}$ in the appropriate bin, and the relevant volume is now a pair of slabs each with volume $L^2\Delta r_{\parallel}$, where $L$ is the cube side length.

Finally, $g_{\perp}(r_{\perp})$ is an indicator of the structure within the smectic layers (see Fig. 6). The separation $r_{\perp}$ is the projection of $r$ onto the plane perpendicular to the director (that is, $r_{\perp}=|\mathbf{r}-\mathbf{r}\cdot\hat{\mathbf{n}}|$). The volume needed is now a cylindrical shell so that

$$g_{\perp}(r_{\perp})=\frac{1}{N\rho}\sum_i \sum_{j\neq i} \frac{\delta(r_{\perp}-r_{\perp,ij})}{\pi L[(r_{\perp}+\Delta r_{\perp})^2-r_{\perp}^2]}. \tag{44}$$

For the smectic $A$ phase, $g_{\perp}(r_{\perp})$ looks much like $g(r)$ for the $I$ phase, indicating a purely liquid-like structure in the smectic layers. For the smectic $B$ (Sm $B$) phase, regular peaks show the onset of hexatic ordering, the degree of which is quantified by $\Psi$.

We generally initialize the system with the molecules on the sites of a face-centered-cubic (fcc) lattice. We allow the lattice structure to melt and then gradually bring the system to equilibrium in the desired phase ($I$, $N$, or Sm $A$ or $B$). This equilibration process can take a large amount of computation time. To facilitate the suggested projects, we have produced a set of pre-equilibrated configurations that are described in the Table and can be downloaded from the *Computers in Physics* FTP server.

The translational and rotational temperatures are calculated as $(1/3N)\Sigma_{i\alpha}p_{i\alpha}^2$ and $(1/3N)\Sigma_{i\alpha}S_{i\alpha}^2/I_{\alpha}$, respectively, and the pressure is $(1/3V)(\Sigma_{i\alpha}p_{i\alpha}^2+\Sigma_{ij}\mathbf{r}_{ij}\cdot\mathbf{F}_{ij})$. (The virial $\Sigma_{ij}\mathbf{r}_{ij}\cdot\mathbf{F}_{ij}$ needs to be obtained within the force-calculation routine.[10]) All these thermodynamic quantities can be calculated from the positions, orientations, and momenta, but we include initial values here to assist readers in checking their own codes.

For each phase, runs should last about 1000 time steps, and sample data should be taken approximately every 10 steps. If access to a vector or parallel machine is available, much longer runs are possible, but 1000 steps should be achievable in a reasonable amount of time on a personal computer and generate useful data.

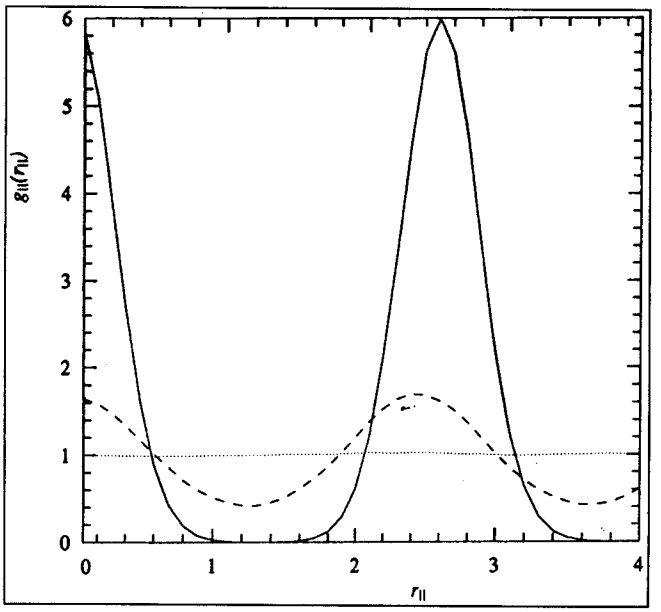


*Figure 5. The distribution function parallel to the director for the nematic (· · ·), smectic A (– – –), and smectic B (—) phases.*

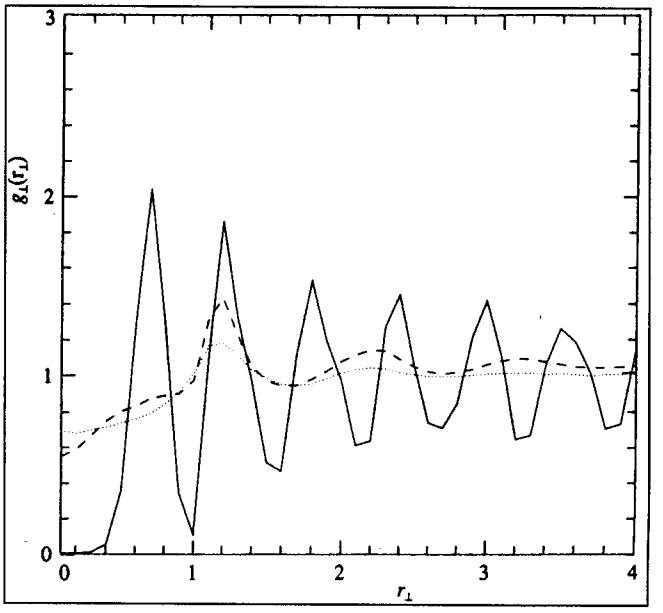


*Figure 6. The distribution function perpendicular to the director. The plot style is the same as in Fig. 5.*

Computer simulations have shed much light on the behavior of liquid crystals, especially with respect to the influence of molecular shape and interactions on observed macroscopic behavior. The Gay–Berne model has proven to be useful in understanding the role of the attractive and repulsive interactions and can be extended beyond the original form discussed here to include dipolar interactions, mo-

lecular chirality,[17] and flexibility. As is well known, liquid crystals are often used in display devices; for example, notebook-computer displays. The molecular alignment induced by the surfaces of these devices is crucial to their operation, and the Gay–Berne model has been used to study such effects.[18] We expect to see many more future studies of extended Gay–Berne models with the aim of understanding basic liquid-crystal physics as well as technologically useful behavior.

## Acknowledgments

This work was supported by the National Science Foundation under Grant No. DMR-9528092. Computational work in support of this project was performed at the Theoretical Physics Computing Facility at Brown University.

## Problems for further study

(1) For each phase, compute $\hat{\mathbf{n}}$, $S$, and $\Psi$. In the $I$ phase, $\hat{\mathbf{n}}$ will fluctuate randomly, whereas in the ordered phases, it will fluctuate about a fairly well-defined average. Note that depending on how you calculate $\hat{\mathbf{n}}$ (the use of a LAPACK routine such as SSYEV is recommended), you may obtain $\hat{\mathbf{n}}$ for one sample and $-\hat{\mathbf{n}}$ for the next.

(2) For each phase, obtain the radial distribution functions $g(r)$, $g_{\parallel}(r_{\parallel})$, and $g_{\perp}(r_{\perp})$. You should be able to see clear differences between the phases including a strong periodicity in $g_{\parallel}(r_{\parallel})$ for the smectic phases, a much more complex structure for $g(r)$ in the nematic and smectic phases compared to the isotropic phase, and a more complex structure for $g_{\perp}(r_{\perp})$ in the Sm $B$ phase compared to the Sm $A$ phase. Note that the periodicity in $g_{\parallel}(r_{\parallel})$ is less than the length of the molecules themselves (recall $\sigma_e = 3$). What does this behavior tell you about the structure of the layers? (Hint: see the caption to Fig. 1.)

(3) Visualization of the configurations can be helpful. Simple views using arrows to represent the molecules can be obtained using programs such as Mathematica or Tecplot. Fancier representations require something like Iris Explorer. If you have access to any of these programs, generate images of the configurations and observe the clear differences in their structures.



## References


1. P. M. Chaikin and T. C. Lubensky, *Principles of Condensed Matter Physics* (Cambridge University Press, Cambridge, 1995).
2. P. G. de Gennes and J. Prost, *The Physics of Liquid Crystals* (Clarendon Press, Oxford, 1993).
3. M. R. Wilson, "Molecular dynamics simulations of flexible liquid crystal molecules using a Gay–Berne/Lennard-Jones model," J. Chem. **107**, 8654 (1997).
4. S. C. McGrother, A. Gil-Villegas, and G. Jackson, "The liquid-crystalline phase behavior of hard spherocylinders with terminal point dipoles," J. Phys.: Condens. Matter **8**, 9649 (1996); "Chain and ring structures in smectic phases of molecules with transverse dipoles," Chem. Phys. Lett. **269**, 441 (1997).
5. P. A. Lebwohl and G. Lasher, "Nematic-Liquid-Crystal Order—A Monte Carlo calculation," Phys. Rev. A **6**, 426 (1972).
6. D. Frenkel, *Phase Transitions in Liquid Crystals*, edited by S. Martellucci and A. N. Chester (Plenum, New York, 1992).
7. J. G. Gay and B. J. Berne, "Modification of the overlap potential to mimic a linear site-site potential," J. Chem. Phys. **74**, 3316 (1981).
8. E. De Miguel, L. P. Rull, M. K. Chalam, and K. E. Gubbins, "Liquid crystal phase diagram of the Gay–Berne fluid," Mol. Phys. **74**, 405 (1991).
9. H. Zewdie, "Computer-simulation studies of diskotic liquid crystals," Phys. Rev. E **57**, 1793 (1998).
10. M. P. Allen and D. J. Tildesley, *Computer Simulations of Liquids* (Clarendon, Oxford, 1987).
11. A. Bulgac and M. Adamuţi-Trache, "Molecular dynamics of rigid molecules," J. Chem. Phys. **105**, 1131 (1996).
12. H. Goldstein, *Classical Mechanics* (Addison-Wesley, Reading, MA, 1980).
13. G. R. Luckhurst, R. A. Stephens, and R. W. Phippen, "Computer simulation studies of anisotropic systems XIX. Mesophases formed by the Gay–Berne model mesogen," Liq. Cryst. **8**, 451 (1990).
14. In the interests of clarity, we have modified the notation somewhat from what is common in the research literature.
15. M. Svanberg, "An improved leap-frog rotational algorithm," Mol. Phys. **92**, 1085 (1997).
16. M. P. Allen, "Simulations using hard particles," Philos. Trans. R. Soc. London, Ser. A **344**, 323 (1993).
17. R. Memmer, H.-G. Kuball, and A. Schönhofer, "Computer simulation of chiral liquid crystal phases III. A cholesteric phase formed by chiral Gay–Berne atropisomers," Mol. Phys. **89**, 1633 (1996).
18. Z. P. Zhang, A. Chakrabarti, O. G. Mouritsen, and M. J. Zuckerman, "Substrate-induced bulk alignment of liquid crystals," Phys. Rev. E **53**, 5 (1996).